Determination of the Sum of the Electric and Magnetic Polarizabilities of the Pion using Polarized Quasi-Real Photons

(Letter of Intend)

R. A. Lindgren, B. E. Norum, B. Sawatzky, L. C. Smith, and K. Wang
University of Virginia, Charlottesville, Virginia

R. S. Hicks, D. Lawrence, R. A. Miskimen
University of Massachusetts, Amherst, MA

L.V. Fil'kov
Lebedev Physical Institute, Moscow,Russia

M. Khandaker, V. Punjabi, and C. Salgado
Norfolk State University, Norfolk, Virginia

A. Afanasev
Jefferson Lab, Newport News, Virginia

November 2002

Abstract

We intend to perform an experiment to determine the sum of the electric and magnetic polarizabilities of the charged pion by measuring pion photoproduction, $\vec{\gamma}p \to \gamma\pi^+n$. The experiment will be performed using a liquid hydrogen target and the proposed quasi-real photon source by means of small Q^2 electroproduction in Hall B. In combination with the comprehensive acceptance and good resolution of CLAS, it will permit the sum of the pion polarizabilities $(\alpha + \beta)$ to be extracted with good precision. With an upgrade for a forward π^+ detector, it would be possible to measure the difference of the pion polarizabilities $(\alpha - \beta)$.

1 Introduction

Electric (α) and magnetic (β) intrinsic polarizabilities characterize the induced transient dipole moments of hadrons subjected to external electromagnetic fields. They are a measure of the rigidity of the internal structure of baryons and mesons, as directly probed, for example, in $\gamma-$hadron Compton scattering. As such, polarizabilities are fundamental quantities predicted by models of hadrons. Due to its light mass and the relative simplicity of the $q\bar{q}$ system, the polarizabilities of the pion are especially important. Indeed, calculations for the pion have been performed using a variety of models, such as the work of Bernard, Hiller, and Weise[1] emphasizing vector meson dominance diagrams, and Bernard et al. [2] within generalized SU(3) models. Another theoretical approach of DSR (dispersion sum rules) is derived at finite energy [3] and at fixed $u = \mu^2$ [4]. For the $\gamma - \pi$ interaction at low energy, Chiral Perturbation Theory (ChPT) provides a rigorous way to make predictions, because it is obtained directly from QCD and relies only on the solid assumptions of spontaneously broken $SU(3)_L \times SU(3)_R$ chiral symmetry, Lorentz invariance, and low momentum transfer [5].

Experimental determinations of the pion polarizabilities are especially challenging since no stable target is available, and indirect processes are required. Moreover, background contributions are always present. For charged pions, three experimental methods have been used: radiative pion-nucleon scattering $\pi N \rightarrow \pi N \gamma$, pion photoproduction in photon-nucleon scattering $\gamma N \rightarrow \gamma N \pi$, and $\gamma\gamma \rightarrow \pi\pi$ as observed in e^+-e^- colliding interactions. Nevertheless, due to background uncertainties and model dependence in the analysis procedures, existing results lack consistency and are generally imprecise.

Chiral symmetry is a property of QCD manifested in the low energy interactions of hadrons. In this domain it has enjoyed much success, and, most particularly for the lightest hadron, the pion, is expected to give reliable predictions for the polarizabilities. Indeed, any disagreement would raise serious questions about our understanding of low-energy QCD [6]. In the chiral symmetry limit of zero quark mass, ChPT predicts the electric and magnetic

polarizabilities of the charged pion to be

$$\bar{\alpha}_E^{\pi^\pm} = -\bar{\beta}_M^{\pi^\pm} = (2.8 \pm 0.5) \times 10^{-4}\mathrm{fm}^3.$$

Most experimental determinations have failed to confirm this prediction. In view of the close connection between ChPT prediction and the underlying validity of QCD, any discrepancy would be considered serious. As emphasized by Holstein [7], "*indeed if QCD is the correct model for the interactions of quarks and gluons then the low energy predictions described here which are predicted on chiral symmetry must obtain. Correspondingly if a strong violation of one or more of these predictions is confirmed, it will be very difficult to reconcile with QCD. Thus the stakes are high and this makes such tests all the more interesting and important*".

We are proposing an experimental test of the π^+ polarizabilities by measuring $\gamma p \to \pi^+ n\gamma$ scattering with photons derived from the low Q^2 electroproduction photon source. The experiment will be most sensitive to the polarizability sum $\bar{\alpha} + \bar{\beta}$. As with the ChPT predictions noted above, all existing theoretical treatments indicate that this sum should be close to zero, however these predictions have never been adequately tested. The proposed investigation will complement experiments planned at CERN, Frascati, and at Mainz. Possibly, with an additional charged pion detector at the forward direction, the difference of the pion polarizability can be measurement.

2 Theoretical Models

Polarizability is a classical concept which describes the extent to which a system is polarized in the presence of an external electromagnetic field. When an external electric field $\vec{E}$ induces an electric dipole moment

$$\vec{p} = 4\pi\alpha\vec{E} \ ,$$

the constant α is identified as the electric polarizability. Similarly, the magnetic polarizability β is defined by

$$\vec{\mu} = 4\pi\beta\vec{H}.$$

In an atomic system, for example, the electric and magnetic polarizabilities are directly related to the index of refraction, which describes forward photon scattering. Therefore, the polarizabilities can be investigated by means of Compton scattering. Traditionally, the polarizabilities have been split into an intrinsic contribution, α or β, given by the sum over all possible dipole transitions to excited states, and an additional term, $\Delta\alpha$ or $\Delta\beta$, representing recoil, retardation, and relativistic effects[5], *e.g.*

$$\bar{\alpha} = \alpha + \Delta\alpha \ .$$

In non-relativistic theory, the latter term is determined by the electric rms radius of the pion,

$$\Delta\alpha = (\alpha_e/3\mu) < r_\pi^2 > \approx 15 \times 10^{-4} \text{ fm}^3,$$

where α_e is the fine structure constant and μ the pion mass. The recoil term $\Delta\alpha$ is positive and if, according to some models, it is larger than values predicted for $\bar{\alpha}$, the intrinsic electric polarizability should be negative[6]. This is speculated to arise from negative-energy intermediate states involving quark sea components[8] in the pion wave function and from disconnected diagrams for the dissociation of a photon into a particle-antiparticle pair. Holstein[6] has associated a sizable negative intrinsic polarizability with vector meson contributions, noting that meson exchange via an axial meson pole diagram provides the essential contribution to the polarizability. Various theories predict rather different values for the pion polarizabilities. For example, an early

evaluation of the polarizability difference $\bar{\alpha} - \bar{\beta}$ by application of the dispersion sum rule (DSR) at finite energy[3] gave $(\bar{\alpha} - \bar{\beta})_{\pi^\pm} = 10.6 \times 10^{-4}$ fm^3. This is consistent with the DSR result of $(\bar{\alpha} - \bar{\beta})_{\pi^\pm} = 10.9 \times 10^{-4}$ fm^3 obtained at a fixed value of the Mandelstam variable $u = \mu^2$[4], but disagrees strongly with the result of a calculation in the linear σ-model with quarks and vector mesons which gave[1]

$$(\bar{\alpha} - \bar{\beta})_{\pi^\pm} \approx 20 \times 10^{-4} \text{ fm}^3.$$

An even larger value was obtained in the Nambu-Jona-Lasinio model[2], leading to the conclusion that the polarizability should be essentially described by the classical finite size term, $\bar{\alpha}_{\pi^\pm} \approx \Delta\alpha$. ChPT has been particularly successful in describing low energy hadronic properties, and provides a firm prediction of the pion polarizabilities. If this prediction were shown to be in error, grave concerns would be raised regarding the validity of low-energy QCD[7]. Because it is obtained directly from QCD and relies only on the fundamental assumptions of spontaneously broken $SU(3)_L \times SU(3)_R$ chiral symmetry, ChPT provides rigorous predictions for the $\gamma - \pi$ interaction at low energy. Unitarity is achieved by adding low-order pion loop corrections, and the resulting infinite divergences are absorbed into physical (renormalized) coupling constants[9, 10]. By means of a perturbative expansion of momenta and quark masses, the method establishes relationships between different processes. For example, at order $\mathcal{O}(p^4)$ the charged pion polarizabilities are simply related to radiative pion beta decay $\pi^+ \to e^+ \nu_e \gamma$ by[10]

$$\frac{\alpha_e h_A}{\sqrt{2} F_\pi \mu} = \bar{\alpha} = -\bar{\beta} = (2.8 \pm 0.5) \times 10^{-4} \text{ fm}^3 \ , \tag{1}$$

where $F_\pi = 93.1$ MeV[11] is the pion decay constant, $h_A = (0.0117 \pm 0.0020)\mu^{-1}$ is the axial vector coupling constant, and α_e is the fine structure constant. In the ChPT predictions, contributions of negative sign to the intrinsic polarizability cancel positive contributions from vector mesons to the finite size terms,[12, 13] leaving only the relatively small component belonging to axial mesons[6].

Beginning at order $\mathcal{O}(p^6)$, additional terms appear in Eq. 1. For example, at order $\mathcal{O}(p^6)$, ChPT predicts a polarizability sum of

$$(\bar{\alpha} + \bar{\beta})_{\pi^\pm} = 0.3 \times 10^{-4} \text{fm}^3 \ ,$$

compared to the null result obtained at $\mathcal{O}(p^4)$. It remains to be shown whether the cumulative effect of $\mathcal{O}(p^6)$ and higher-order corrections modify the $\mathcal{O}(p^4)$ predictions significantly. The convergence properties of ChPT are tested more conclusively with the pion. Dispersion sum rules have also been utilized to predict pion polarizabilities. For charged pions, for example, $s-$channel ($\gamma\pi \to \gamma\pi$) and t-channel ($\gamma\gamma \to \pi\pi$) analyses[3, 4] give

$$\bar{\alpha} + \bar{\beta} = (0.39 \pm 0.04) \times 10^{-4} \text{ fm}^3,$$

and

$$\bar{\alpha} - \bar{\beta} = 10.8 \times 10^{-4} \text{ fm}^3,$$

implying $\bar{\alpha} = 5.6$ and $\bar{\beta} = -5.2$. Because of the difficulties in evaluating the high-energy asymptotic contributions, these results are model-dependent. Pion polarizabilities have also been evaluated in the Dubna quark confinement model[14], with the result $\bar{\alpha} = 3.63$. These and other predictions are listed in Table 1. Whereas varying values are obtained for the individual electric and magnetic polarizabilities, the different theories concur that the sum of the polarizabilities $\bar{\alpha}_\pi + \bar{\beta}_\pi$ of the charged pion should be small. The reason for this is that the lowest order contributions of the internal structure to an effective Lagrangian depend on the electromagnetic fields E and B according to $\mathcal{L}_{eff} \sim F_{\mu\nu}F^{\mu\nu} \sim E^2 - B^2$, hence $\bar{\alpha} = -\bar{\beta}$ [7]. All higher order contributions involve additional gradients in the Lagrangian, *i.e.* momenta and mass terms, which are small near threshold due to the small mass of the pion.

3 Experimental Results

In the absence of a free pion or photon target, experimental studies of pion polarizability must be made indirectly, relying on virtual target particles. For example, with an incident beam of real photons, the elementary Compton scattering process shown as Fig. 1a can be accessed as one of the two vertices of the diagram represented in Fig. 1b, where the target is a virtual pion in the pion field of a proton. At small values of $|t|$, the squared invariant mass of the virtual pion, the interaction takes place at a relatively large distance from the proton, and is mediated by a single pion. The reaction represented by Fig. 1b can be measured over a wide kinematic range, and, in principle, all three final products can be detected. Although this aids the separation of the two vertices, the desired cross section lies at the pion pole in an experimentally inaccessible region, and recourse is needed to a model-dependent extrapolation procedure, such as the Chew-Low[15] method.

In an alternative method of radiative pion scattering, an incident high-energy pion scatters from a virtual photon in the electromagnetic field of a nucleus, as represented in shown in Fig. 1c. In this case[16] extrapolation is also required, however, in an entirely physical parameter, the four-momentum squared: $Q^2 \to 0$. The primary disadvantage of this technique is the large hadronic backgrounds: Compton scattering is electromagnetic, whereas the interaction of the pion with the target is predominantly by means of the strong force.

Compton scattering from the pion also occurs in high-energy e^+-e^- collisions, by means of the reaction $\gamma\gamma \to \pi^+\pi^-$ represented in Fig. 1d. The Compton amplitude in this case is obtained by crossing symmetry. At threshold the reaction depends heavily on the s-wave $\pi - \pi$ interaction, and the threshold cross section is modeled by fitting data in the kinematic region $S_1 < -\mu^2$ and $t_1 > 4\mu^2$, where s_1 and t_1 are the square of the total energy, and the momentum transfer in the $\gamma\pi$-channel, respectively. The result of this fit is then extrapolated to the point $S_1 = \mu^2$, $t_1 = 0$ of the reaction $\gamma\pi \to \gamma\pi$ in order to determine the pion polarizabilities. The extrapolation is over a large range and model-dependent[17].

All three methods outlined above have been exploited. For example, pion photoproduction was measured[18] at the Lebedev Institute with bremsstrahlung photons ranging from 350 to 800 MeV. All three final products, γ, π^+, and n were detected using small solid-angle detectors. There was no tracking of charged particles and statistics were limited to 2200 events extracted from 147k raw data events. The deduced electric polarizability, obtained under the assumption $\bar{\alpha} + \bar{\beta} = 0$, was $\bar{\alpha} = (20 \pm 12) \times 10^{-4}\text{fm}^3$.

Radiative pion scattering was measured[19, 20] at Serpukov with a 40 GeV π^- beam on targets of Be, C, Al, Fe, Cu, and Pb. From 2100k raw data events, 7k Compton events were identified over a wide range of photon scattering angles. For photons backward-scattered in the pion rest frame, the polarizability contribution to the Compton cross section is proportional to $\bar{\alpha} - \bar{\beta}$. For forward scattered photons, polarizability contributes as $\bar{\alpha} + \bar{\beta}$. By analyzing data over the extended angular range, Antipov *et al.*[19, 20] obtained

$$\bar{\alpha} - \bar{\beta} = (13.6 \pm 2.8) \times 10^{-4}\text{fm}^3,$$

and

$$\bar{\alpha} + \bar{\beta} = (1.4 \pm 3.1 \pm 2.5) \times 10^{-4}\text{fm}^3 \ .$$

Two-photon interactions have been measured at several facilities, including PLUTO, DM1, DM2, MARK2[21, 22, 23, 24, 25]. Unfortunately, statistics are typically poor and a discrepant range of answers has resulted. Nevertheless, impressive precision has been reported in some of these analyses. For example, assuming $\bar{\alpha} + \bar{\beta} = 0$, Babusci *et al.*[5] extracted a charged pion polarizability of $\bar{\alpha} = (2.2 \pm 1.6) \times 10^{-4}$ fm^3 from data obtained with the MARK2 detector. However, the precision claimed in this result seems unduly optimistic in light of a subsequent theoretical study[10]. Even more striking results have been obtained by analyses of $\gamma\gamma \to \pi\pi$ data that employ dispersion sum rules. For example, from the same MARK2 data, Kaloshin *et al.*[26] derived a value of $\bar{\alpha} + \bar{\beta} = (0.22 \pm 0.06) \times 10^{-4}$ fm^3 for the charged-pion polarizability sum. Such analyses are acknowledged to have considerable model sensitivity, and have received severe criticism. For example, in the DaΦne handbook Portols and Pennington[27] conclude that *the only way to measure the pion polarizabilities is in the Compton scattering process near threshold and not in* $\gamma\gamma \to \pi\pi$.

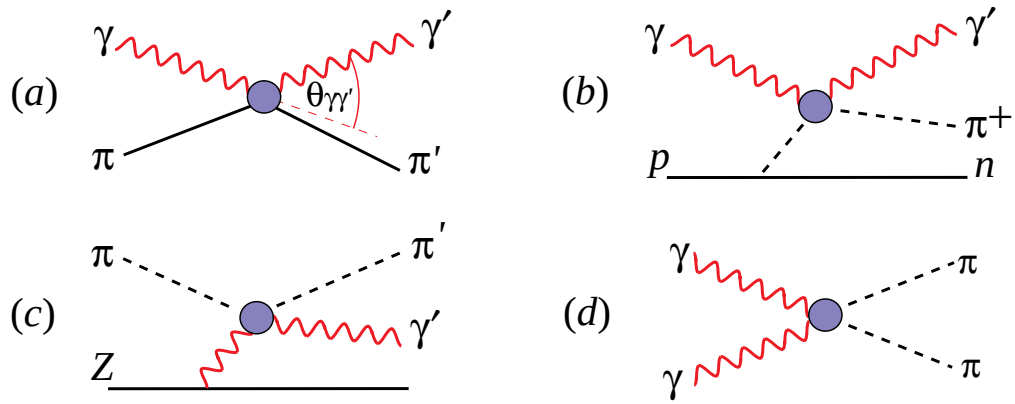

Figure 1: Diagrams for pion Compton scattering. (a) Elementary diagram; (b) radiative pion photoproduction; (c) radiative pion scattering; and (d) diagram for double pion production in two photon scattering.

Model	Data	Reaction	$\bar{\alpha}$ $(10^{-4} fm^3)$	Ref.
ChPT			2.7	[7]
DSR			5.6	[3][4]
Bernard			7-14	[1][2]
	Lebedev	$\gamma p \to \gamma \pi^+ n$	20 ± 12	[18]
	Serpukov	$\pi^- A \to \gamma \pi^- A$	$6.8 \pm 1.4 \pm 1.2$	[19]
	PLUTO	$\gamma\gamma \to \pi^+\pi^-$	$19.1 \pm 4.8 \pm 5.7$	[21]
	DM1	$\gamma\gamma \to \pi^+\pi^-$	17.2 ± 4.6	[22]
	DM2	$\gamma\gamma \to \pi^+\pi^-$	26.3 ± 7.4	[23]
	MARK II	$\gamma\gamma \to \pi^+\pi^-$	2.2 ± 1.6	[24]
	Data	Reaction	$\bar{\alpha} + \bar{\beta}$	Ref.
	Serpukov	$\pi^- A \to \gamma \pi^- A$	$1.4 \pm 3.1 \pm 2.8$	[19]
	Data	Reaction	$\bar{\alpha} - \beta$	Ref.
	Serpukov	$\pi^- A \to \gamma \pi^- A$	13.6 ± 2.8	[19]

Table 1: Measured and calculated pion polarizabilities.

As revealed by the summary presented in Table 1, notwithstanding significant effort, the present experimental information on the polarizabilities of the pion is unsatisfactory. More accurate and reliable determinations are needed to test the precise predictions provided by recent theoretical advances, such as ChPT. Accordingly, a new round of experimental studies has been proposed including radiative pion scattering at COMPASS (CERN) and pion photoproduction using tagged photons at Mainz[28][29]. A measurement of pion photoproduction using tagged polarized photons with CLAS can complement these studies. In particular, the similar experiment at Mainz is configured for backward-scattered photons and will therefore be primarily sensitive to the polarizability difference. On the other hand, with CLAS there is large acceptance to forward-scattered photons, allowing us to greatly improve experimental information on the polarizability sum. The nearly 4π CLAS detector is of considerable benefit in this regard, and the availability of a highly polarized photon beam will enhance the polarizability contribution while, at the same time, suppressing backgrounds.

4 Kinematics and Cross Sections

4.1 Kinematics

The reaction from which we seek to determine the pion polarizabilities is $\vec{\gamma}p \rightarrow \gamma\pi^+ n$. As defined in Fig. 1*b*, the 4-momentum of the incoming photon in the laboratory system is $k_1 = (\vec{k}, k)$, and $k_2 = (\vec{k}', k')$ for the outgoing photon. Other four-momenta are $q = (\vec{q}, E)$ for the pion, $P_1 = (0, M_p)$ for the target proton, and $P_2 = (\vec{P}_2, E_2)$ for the recoil neutron. We set M_p, M_n, and μ to represent the masses of the proton, neutron, and pion. For incident tagged photons, we can reconstruct all kinematics if we know the 4-momenta of any two reaction products. Two other reconstructed variables serve to describe the multi-particle system. The first is the 4-momentum transfer delivered to the neutron. This is equal to the squared invariant mass of the off-shell pion, and is represented by

$$t = (M_n - M_p)^2 - 2T_n M_p, \tag{2}$$

where T_n is the kinetic energy of the neutron. Neglecting the p-n mass difference, t is negative and proportional to T_n. For an on-shell pion, $t = \mu^2$, the location of the pion pole. The variable t specifies the off-shell mass of the struck virtual pion, and it is the variable over which extrapolation is made to obtain the Compton scattering cross section for a free pion. By restricting data to small t, we ensure that the measured reaction is mediated by one-pion exchange. The other variable of importance is S_1, the squared invariant mass of the $\gamma - \pi^+$ system:

$$S_1 = (k' + E)^2 - (\vec{k}' + \vec{q})^2 \ . \tag{3}$$

The lower limit of S_1 is $1\mu^2$, and the higher limit is set by the incoming photon energy. It is convenient to use μ^2 as the unit of t and S_1. From the phase-space of t and S_1, shown in Fig. 2, we see that at constant S_1 higher photon energies give access to the smaller $|t|$-values that are favorable for making reliable extrapolations. Three other independent kinematic variables are S, the squared invariant mass of the initial state, t_1, the 4-momentum transfer delivered to the pion, and S_2, the squared invariant mass of the the

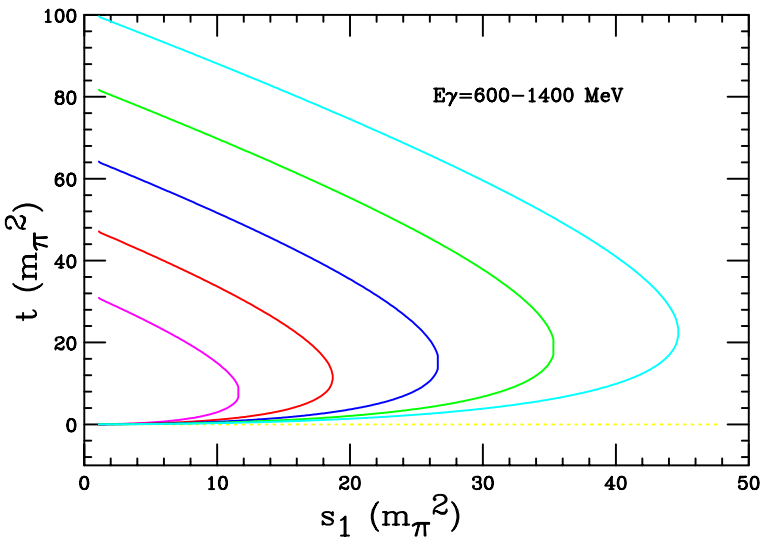

Figure 2: For t-channel pion photoproduction the allowed phase space lies within the contours. The smallest (inner) contour belongs to 600 MeV photons and the largest to 1400 MeV. Contours are indicated for 200 MeV energy increments.

pion-neutron system:

$$\begin{aligned} S &= (k_1 + P_1)^2 \ , \\ t_1 &= (k_2 - k_1)^2 \ , \\ S_2 &= (q + P_2)^2. \end{aligned} \tag{4}$$

4.2 Scattering of Unpolarized Photons from Free Pions

The differential cross section for the Compton scattering of an unpolarized photon from a free charged pion can be written[17]:

$$\begin{aligned} \frac{d\sigma_{\gamma\pi}}{d\Omega} &= \left(\frac{d\sigma_{\gamma\pi}}{d\Omega}\right)_B - \frac{e^2(S1-1)^2}{16\pi \cdot S_1^2[(S_1+1)+(S_1-1)z]} \cdot \\ & \quad [(1-z)^2(\bar{\alpha}-\bar{\beta}) + S_1^2(1+z)^2(\bar{\alpha}+\bar{\beta})] + ... \end{aligned} \tag{5}$$

where $z = \cos\theta_{\gamma\gamma}^{cm}$. The leading-order Born term gives the threshold cross section. This Thomson limit is defined by the charge of the pion. The polarizabilities enter as corrections, beginning with the next term that represents the interference with the Born amplitude. Equation 5 shows that backward scattering, *i.e.* negative z, favors the polarizability difference $\bar{\alpha}-\bar{\beta}$, while forward scattering, *i.e.* positive z, favors the polarizability sum $\bar{\alpha}+\bar{\beta}$. Although the polarizability sum is expected to be small relative to the difference, its contribution is enhanced for S_1 even slightly removed from threshold. The Born cross section depends only on S_1 and the center-of-mass photon scattering angle. For unpolarized photons it is[30]

$$\left(\frac{d\sigma_{\gamma\pi}}{d\Omega}\right)_B = \left(\frac{e^4}{4\pi}\right)^2 \frac{1}{S_1} \frac{(S_1^2+1)(1+z^2)+2(S_1^2-1)z}{[S_1+1+(S_1-1)z]^2}. \tag{6}$$

Fil'kov and Kashevarov suggested [31] that the method of extrapolation of the pion polarizabilities from the $\gamma\pi$ elastic scattering allows the correction to the low energy expression (Eq. 5) to be taken into account.

4.3 Scattering of Linearly-Polarized Photons from Free Pions

When the plane of polarization of an incident linearly-polarized photon beam is in the scattering plane, the Compton cross section is[17]

$$\begin{aligned}\frac{d\sigma_{\parallel}}{d\Omega} &= \left(\frac{e^2}{4\pi}\right)^2 \frac{1}{S_1}\left(1-\frac{2(1-z)}{(S_1+1)+(S_1-1)z}\right)^2 - \frac{e^2}{4\pi}\frac{(S_1-1)^2}{4S_1^2}\times \\ &\left(1-\frac{2S_1(1+z)}{(S_1+1)+(S_1-1)z}\right)\times \\ &\Big[(1-z)(\bar{\alpha}-\bar{\beta})-S_1(1+z)(\bar{\alpha}+\bar{\beta})\Big]+... \end{aligned} \tag{7}$$

For photons polarized perpendicular to the scattering plane the cross section is

$$\begin{aligned}\frac{d\sigma_{\perp}}{d\Omega} &= \left(\frac{e^2}{4\pi}\right)^2 \frac{1}{S_1} - \frac{e^2}{4\pi}\frac{(S_1-1)^2}{4S_1^2}[(1-z)(\bar{\alpha}-\bar{\beta})+ \\ &S_1(1+z)(\bar{\alpha}+\bar{\beta})]+... \end{aligned} \tag{8}$$

As in the case of unpolarized incident photons, the cross section is seen to be sensitive to $\bar{\alpha}-\bar{\beta}$ for backward scattering and to $\bar{\alpha}+\bar{\beta}$ for forward scattering at large S_1. Inspection of these equations further reveals that for a scattering angle given by

$$z = z_0 = -\frac{S_1-1}{S_1+1}, \tag{9}$$

the interference contribution to the cross section for parallel polarization vanishes. For $5 < S_1 < 10$ the corresponding center-of-mass scattering angle varies from 132° to 145°. Measurements at this backward scattering angle could be utilized to check the reliability of the extrapolation procedure and the known Born cross section should be obtained. In principle, higher-order terms such as $\bar{\alpha}^2$ would modify this expectation, but the effect would be difficult to observe. At this same angle z_0, only the electric polarizability $\bar{\alpha}$ contributes to the cross sections for unpolarized photons and for perpendicularly-polarized photons. In principle then, by means of precision measurements at z_0, the electric polarizability of the pion could be

uniquely determined. More generally however, the availability of precision data over an extended range of photon scattering angles $\theta_{\gamma\gamma}^{\rm cm}$ would permit both polarizations, $\bar{\alpha}$ and $\bar{\beta}$, to be determined. This holds *independent* of the polarization properties of the incident photon. Figure 3 shows the angular dependence of the Compton scattering differential cross section for two values of S_1 and various values of $\bar{\alpha}-\bar{\beta}$ and $\bar{\alpha}+\bar{\beta}$; The Born term is represented by $\bar{\alpha}-\bar{\beta}=\bar{\alpha}+\bar{\beta}=0$. Three conclusions may be drawn from these graphs: The polarizability contribution to the cross section increases with increasing S_1; the sensitivity to $\bar{\alpha}+\bar{\beta}$ at forward angles is considerably greater than the sensitivity to $\bar{\alpha}-\bar{\beta}$ at backward angles; and perpendicularly-polarized incident photons are most sensitive to pion polarizability.

A favorable condition to determine $\bar{\alpha}+\bar{\beta}$ hence occurs for perpendicularly polarized photons scattering at relatively forward angles with values of S_1 not too close to threshold. A further advantage of perpendicular polarization, indicated by calculations of Drechsel and Fil'kov[17], is that the contribution of diagrams that constitute a background to the t-channel diagram are decreased. Such an experiment is well-suited to CLAS, especially with the availability of polarized photons from the low Q^2 electroproduction photon source. Moreover, the comprehensive angular acceptance of CLAS provides simultaneous detection of all possible alignments of the photon polarization angle with respect to the scattering plane. The enhanced sensitivity to $\bar{\alpha}+\bar{\beta}$, indicated by Fig. 3, provides a severe test of theoretical notions that $\bar{\alpha}+\bar{\beta}\approx 0$.

4.4 Pion Photoproduction

As previously noted, the free $\gamma-\pi$ scattering cross section is not measured directly, but instead through the reaction $\gamma p\to\gamma\pi^+n$. In the late fifties Chew and Low[15] showed how unstable particles, *e.g.* virtual pions in the pion cloud of a nucleon, could serve as targets for scattering experiments. When $|t|$, the squared invariant mass of the virtual pion, is small, it is relatively distant away from the nucleon, and in interacting with an external particle may gain sufficient energy to escape as a real pion. In order to obtain the free pion cross section an extrapolation in t is needed to the pion pole at $t=+\mu^2$, whereas the physical region accessed in such an experiment is restricted to

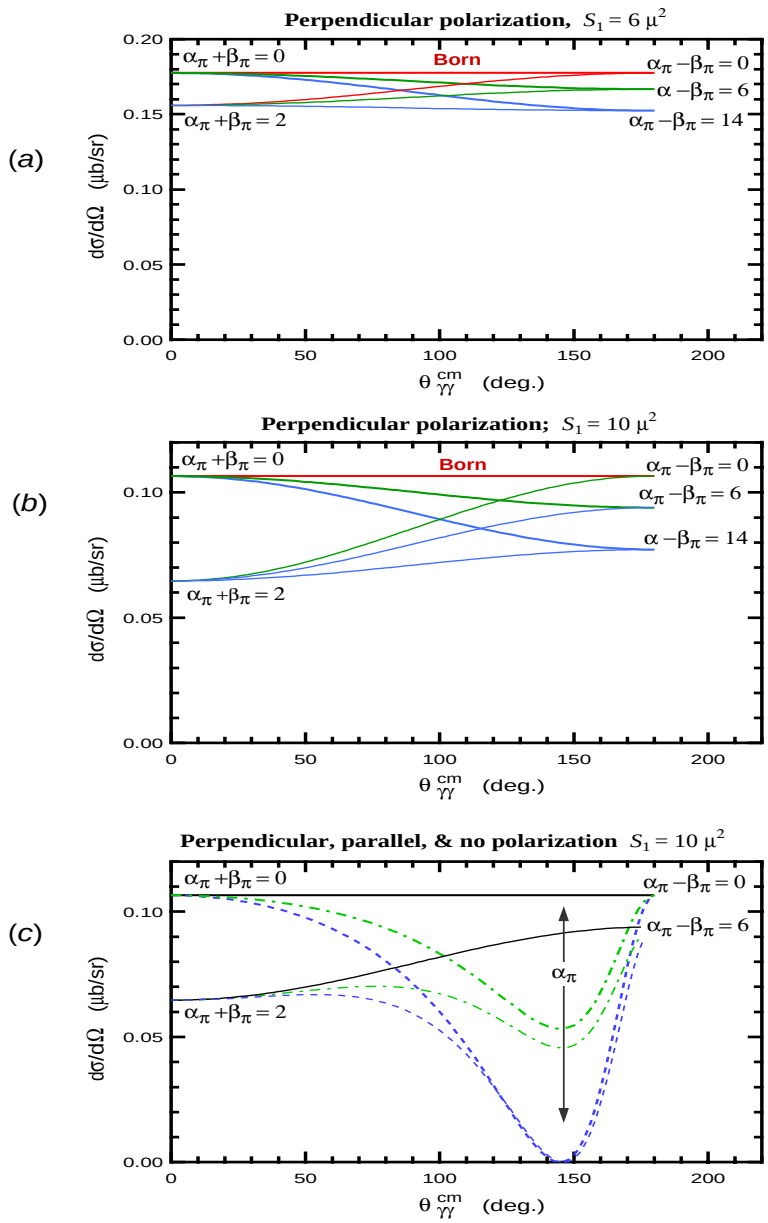

Figure 3: Cross sections for π^+ Compton scattering for different polarization state and S_1. In Fig 3c, the solid curve shows the perpendicular case, the dashed curve shows parallel case, and the dash-dotted the unpolarized case.

$t < 0$. This technique has been successfully employed to determine the pion-nucleon coupling constant through $\gamma p \to \pi^+ p$ reaction[32], as well as from N-N scattering[33]. It is also used in the determination of $\pi\pi \to \pi\pi$ scattering from the $\pi p \to \pi\pi p$ reaction[34]. The method will be also used in JLab experiments 94-105, a chiral anomaly study[35].

In the present case, the Chew-Low relation between the γp and $\gamma\pi$ cross sections may be expressed as[36]:

$$\lim_{t\to 1} \frac{d^3\sigma_{\gamma p\to\gamma\pi N}}{dtdS_1 d\Omega} = \frac{g^2}{4\pi}\frac{(S_1-1)}{8\pi M_p^2 E_\gamma^2}\frac{(-t)}{(t-1)^2}G_A^2(t)(\frac{d\sigma}{d\Omega})_{\gamma\pi\to\gamma\pi} \tag{10}$$

where $g^2/4\pi = 14.7$ is the pion-nucleon coupling constant and the axial form factor of the nucleon $G_A^2(t)$ is normalized to unity at $t = 0$. The γp cross section depends on the $N\pi N$ and $\gamma\pi$ vertices and a t-channel propagator. For the purpose of illustration, we assume that the above relation holds for values of t moved away from the pion pole. The corresponding t-channel cross section is plotted in Fig. 4 as a function of t for $E_\gamma = 700$ MeV and $S_1 = 6$. The cross section passes through zero at $t = 0$, rises to a maximum at $t = -1$, and then decreases. The t-channel cross section is seen to be large near $t = -1$, and very small for $t \approx 0$. Multiplying the γp cross section by the pole term $(t-1)^2$, we define

$$F(t) \;=\; \frac{d\sigma_{\gamma p\to\gamma\pi N}}{dtdS_1 d\Omega} \times (t-1)^2(2E_\gamma M_p)^2 \Rightarrow -\frac{g^2}{8\pi^2}(S_1-1)tG_A^2(t)\left(\frac{d\sigma}{d\Omega}\right)_{\gamma\pi\to\gamma\pi} \tag{11}$$

a straight line passing through the origin. This proportional t-dependence results from the the nature of pseudoscalar one-pion exchange. For a pure t-channel process then, the extrapolation to the pion pole at $t = 1$ simply follows a straight line. At the pole,

$$F(t=1) = -\frac{g^2}{8\pi^2}(S_1-1)G_A^2(t)\left(\frac{d\sigma}{d\Omega}\right)_{\gamma\pi\to\gamma\pi} , \tag{12}$$

and

$$\frac{d\sigma_{\gamma\pi}}{d\Omega} \;=\; -K(S_1, E_\gamma) \times \lim_{t\to 1} F(t) \; , \tag{13}$$

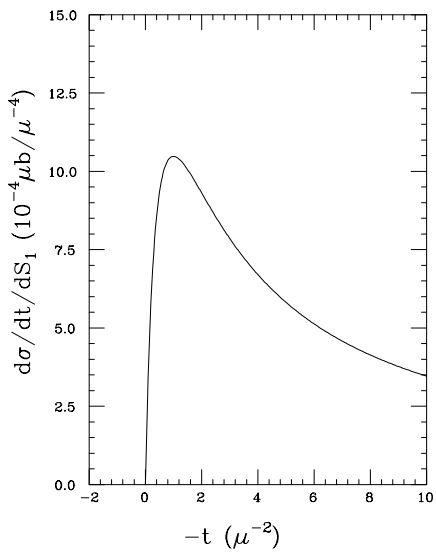

Figure 4: t-dependence of the total cross section in the $\gamma p \to \gamma \pi^+ n$ reaction with pure OPE for $E_\gamma = 0.7$ GeV and $S_1 = 6$.

where

$$K(S_1, E_\gamma) \;=\; \frac{8\pi^2}{g^2(S_1 - 1)} \;. \tag{14}$$

In practice, as the pion moves off the mass shell the two vertices become described by form factors and accordingly $F(t)$ becomes more complicated. Moreover, at larger values of $|t|$ reaction diagrams other than the t- channel process contribute, such as s-channel, u-channel, and two-pion exchange. Calculations of these processes are model-dependent.

4.5 Extraction of Pion Polarizability

Reliable extrapolation demands the availability of statistically precise data extending to values of $-t$ that are as close to zero as possible. As indicated in Fig. 2, the lower limit of $-t$ accessible in this experiment is set by the photon energy and S_1. The t-channel cross section has been shown to reach a maximum at $t = -1$, for which the kinetic energy of the recoil neutron is approximately 10 MeV. Much smaller values of $-t$ are difficult to access because the neutron kinetic energy diminishes and the range of the time-of-flight TDCs precludes the detection. Small values of $-t$ are best measured at higher photon energies; however, count rates decrease since the cross section is proportional to $1/{E_\gamma}^2$. Also demanding care is the presence of singularities in the extrapolation path. These singularities can be removed by integrating the function $F(t)$ over ϕ from 0 up to 2π and over θ from 120 up to 160° for the back scattering experiment and from 20 up to 60° for the forward one The comprehensive acceptance of CLAS makes this requirement easy to meet. Figure 5 shows an example of quality of data expected in this experiment, as well as the results of two linear extrapolation fits.

Much effort has been invested to test the reliability of the extrapolation procedure. Here we will briefly summarize the findings. Pseudodata, generated in the physical $-t$ region using a variety of models, have been extrapolated to the pion pole using polynomial expansions and Pade approximation of various orders. The extrapolation error is determined from the error matrix for the extrapolation fit. These simulations show that the extrapolation is reliable *provided it is made over a region in t for which the function $F(t)$ remains close to linear.*

When curvature in $F(t)$ dictates fitting with a quadratic polynomial or Pade approximation, the extrapolation becomes unreliable: not only does the extrapolation uncertainty increase markedly, but the pole cross section of the generating function is not reproduced within this magnified error. Just how linear is the function $F(t)$ in the region of extrapolation? As has been shown, if only the t-channel diagram were present, $F(t)$ would be perfectly linear. Because only published data[18] in this region are uninstructive due to very large statistical errors, one turns to the theoretical evaluations of

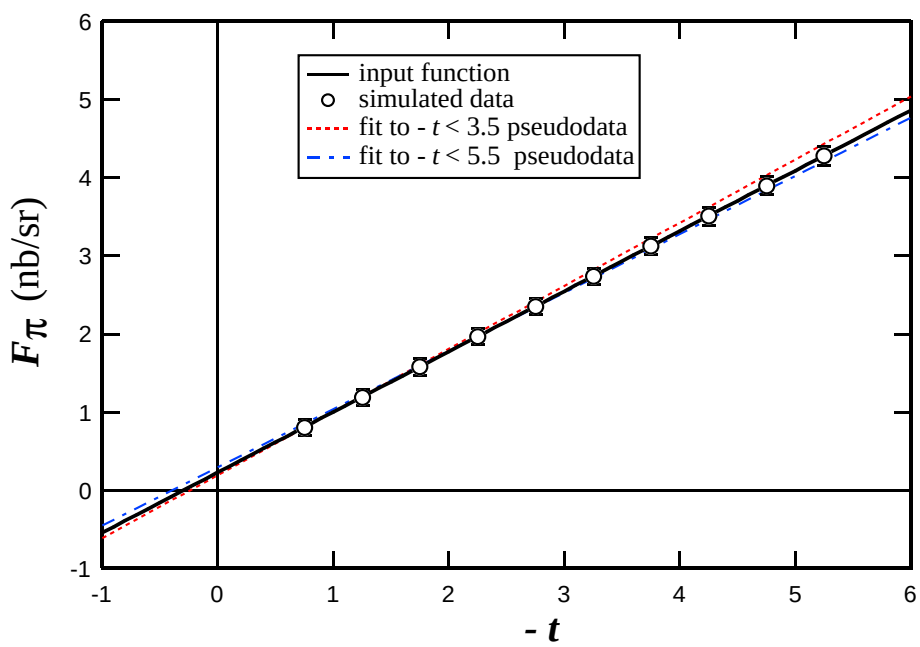

Figure 5: Simulated extrapolation using generated data having the statistical accuracy projected for the kinematic range $7 < S_1 < 8$. The solid curve is the assumed input function, the dashed and dash-dotted curves show fits and extrapolations for two limits of t. Both S_1 and t are in units of the pion mass squared.

Fil'kov[28][29], which include many of the important background diagrams. An example of these calculations, shown in Fig. 6 indicates that $F(t)$ remains close to linear up to $-t = 3.5$. More detailed calculations recently made suggest that the linearity persists up to at least $-t = 5$. We have found that a 10% quadratic change over the fitting range introduces an uncertainty in the extracted polarizability parameter that is comparable to the overall statistical uncertainty. However, to date calculations have been made only for backward photon scattering, not for the forward-scattering that is the emphasis of this proposal. In any case, whatever the kinematics, the t-dependence of $F(t)$ can only be confirmed by experiment. On the other hand, the real F(t) could be non-linear. To handle this function close to the linear one, some method of a conformal mapping of the analytic region of the scattering amplitude can be used. However, such methods are effective only if the experimental measured region of t is essentially more than the extrapolation region. Therefore, it is desirable to have $-t > 10$.

An alternative way to investigate the pion polarizability is suggested by Fig. 6. This shows the polarizability contribution to the cross section in the physical region for $S_1 = 6$. The data will be simultaneously acquired throughout this comprehensive range in S_1. The low-S_1 results can be used to test and refine the best available theoretical evaluations of threshold pion photoproduction. Observed departures from these predictions at large S_1 could be used to assess any polarizability contributions.

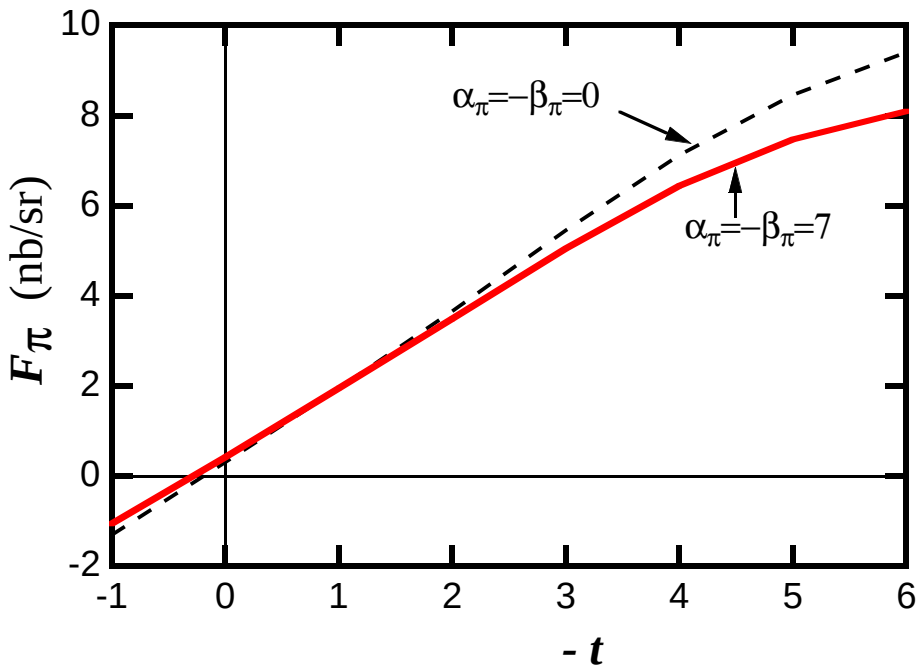

Figure 6: Calculated[28][29] reduced cross sections for $S_1 = 6$ and $\theta^{\rm cm}_{\gamma\gamma} = 140 - 180^\circ$ by integration over ϕ. The dashed line is the Born result.

5 CLAS Experiment

This measurement of $\vec{\gamma}p \rightarrow \gamma\pi^+n$ requires polarized photons generated from 3.2 GeV electron beam, a liquid hydrogen target, and CLAS.

5.1 Photon Source

Even after the data are binned with respect to various kinematic parameters such as S_1, good statistical precision is mandatory for a reliable extraction of the pion polarizability. Furthermore, since we seek to measure by time-of-flight a relatively slow neutron in the final state, the experiment has acute sensitivity to background. These two requirements demand a photon source that has very high tagging efficiency and is quite background-free. The proposed small Q^2 electroproduction photon source will be used for this purpose. As described in [37], electroproduction at very small Q^2, which corresponds to those electrons scattered at very forward angles around 1°, can be used as a photon source to generate a partially linear polarized photon beam.

The polarization of the photon source is a function of the photon energy. For a 3.2 GeV electron beam, the linear polarization will be better than 90% at 0.7 GeV. In comparison to the coherent photon source, the new quasi-real photon source can provide the same polarization while the flux will be doubled.

There are two backgrounds which generate small angle scattering events. The first one is Bremsstrahlung radiation which is peaked at much smaller angles, less than 0.5°. The second one is Moller electron scattering which is minimized between 0.5 and 1.4°. Therefore, by carefully controlling of the electron scattering angles, these two background can be suppressed effectively.

We plan to run the experiment at relatively lower photon energies for several reasons. Firstly, the total t-channel cross section is in reciprocal proportion to beam energy. Hence lower energy will offer more counts. Secondly, at low energy, it will be possible to catch some forward pions in the laboratory

system originated from the backward $\gamma\pi^+$ scattering. This will help us to obtain information about $\alpha - \beta$. Thirdly, aiming at lower photon energy, we could get higher photon flux as well as better polarization. Finally, at lower energy, we could have better missing mass resolution to separate the Compton events from π^o production.

5.2 Particle Detection

The minimum requirements for event reconstruction are a tagged photon, a positively-charged pion, and a recoil neutron in the TOF counter. Although this information is adequate to reconstruct the entire reaction kinematics, the 300 to 600 MeV photons scattered at relatively forward angles may also be detected in the forward-angle electromagnetic shower counter, albeit with mediocre resolution. This provides valuable independent checks on the kinematic reconstructions and background rejection.

For the selected kinematics, the momentum of the pion ranges from 250 to 600 MeV/c. A magnetic field of one-third to one-half the nominal torus field value provides good acceptance and momentum reconstruction for such pions. Pions will be detected in the start counter and tracked through the drift chambers to the TOF counter, where they can be identified from other charged particles by TOF. In principle, neutrons can be detected in either the TOF counter or electromagnetic calorimeters. However, for this experiment, the 10 to 60 MeV kinetic energy of the neutrons is inadequate to exceed the calorimeter threshold. The TOF counter consists of long scintillator bars situated about 5 meter from the target. These bars are 20 cm wide and 5 cm thick, and light is collected by photomultiplier tubes at each end. From the time difference of the two signals, the azimuthal angle will be given to better than 1° resolution. Similarly, the polar angle is established to about 1° by the position of the hit scintillator bar. The TOF scintillators have about 10% detection efficiency for neutrons in this energy range. This detection efficiency can be precisely calibrated by analyzing $\gamma d \to pn$ or $\gamma p \to \pi^+ n$ data. The neutron energy resolution relies on the timing resolution of the TOF counter, $\sigma \approx 150$ ps. With such precision, 1% energy resolution can be expected for neutrons of 10 to 60 MeV, corresponding to a resolution 1 % in

t. Finally, the FWHM resolution of the tagged photon beam is assumed to be 2 MeV.

5.3 Kinematic Resolutions and Acceptances

Event kinematics were generated for photon energy $k = 700$ MeV, $0.5 < -t < 6$, $4 < S_1 < 10$, and $0° < \theta_{\gamma\gamma}^{\rm cm} < 180°$. The response of CLAS for these events was then simulated using the SDA code[38]. Figure 7 shows the calculated missing mass spectrum. By virtue of the excellent resolution for the pion and recoil neutron, the FWHM missing mass resolution is less than 0.002 GeV^2, much smaller than 0.018 GeV^2, the square of the pion mass. This favors the rejection of potential backgrounds from two-pion production. Figure 8 indicates the corresponding resolution for S_1, less than 1 μ^2. Good resolution in S_1 is important for evaluating the Born term contribution to the Compton cross section. Figures 9-11 show the calculated acceptances as functions of t, S_1, and the center-of-mass scattering angle $\theta_{\gamma\gamma}^{\rm cm}$. All these plots include an assumed neutron detection efficiency of 10%. The lower limit of the neutron kinetic energy was set around 10 MeV, corresponding to a flight time of 120 ns. Because the available range of the TDC extends to 150 ns and the discriminator threshold is ≈ 1.5 MeV, < 10 MeV neutrons can be measured in practice, corresponding to events with $-t < 1$.

Of particular importance for event reconstruction is the precise measurement of the π^+ that CLAS provides. However, for backward photon scattering, $\theta_{\gamma\gamma}^{\rm cm} \approx 180°$, pions recoil at small angles relative to the beam direction and are not detected in CLAS. Hence, as seen in Fig. 11, the acceptance for large $\theta_{\gamma\gamma}^{\rm cm}$ is poor. Conversely, for forward-scattered photons the recoil pions are efficiently detected and the acceptance is high. For the kinematic range of interest the recoil neutrons have relatively low kinetic energies, favoring precise momentum measurements by time-of-flight. The photon angular distribution is found to span a large range. Most easily measured in the calorimeter will be the highest energy photons that result from forward scattering.

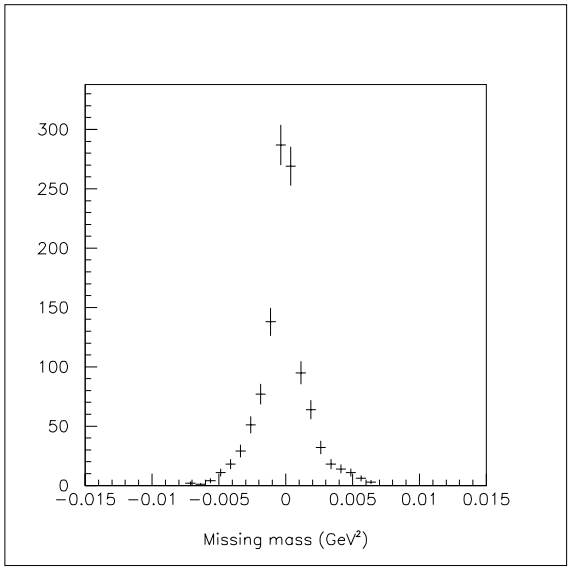

Figure 7: Missing mass spectrum for the reconstruction of the scattered photons. The results are for 700 MeV incident photons, $-t = 2.5$, $S_1 = 6.0$, and $\theta_{\gamma\gamma}^{\rm cm} = 20^\circ$.

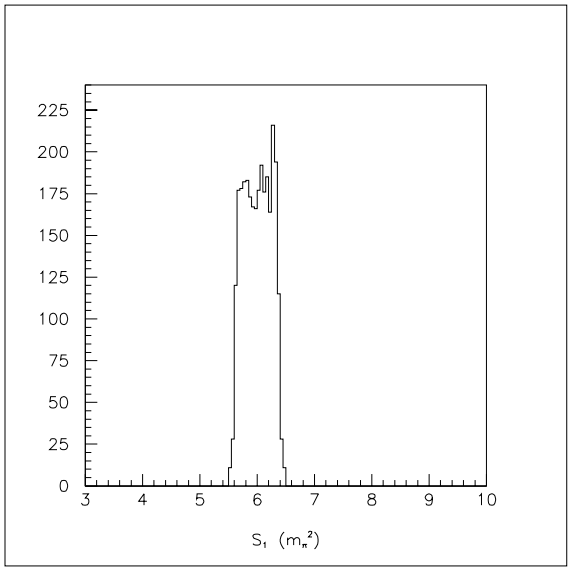

Figure 8: S_1 resolution for $k = 700$ MeV, $-t = 2.5$, $S_1 = 6.0$, and $\theta_{\gamma\gamma}^{\rm cm} = 20°$.

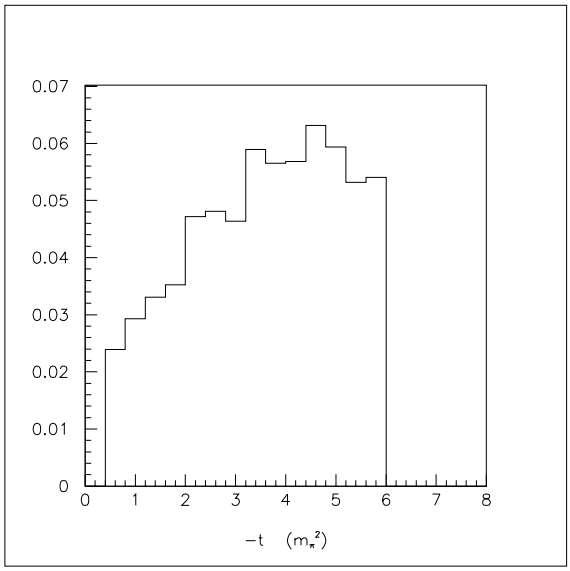

Figure 9: t acceptance for 700 MeV incident photons.

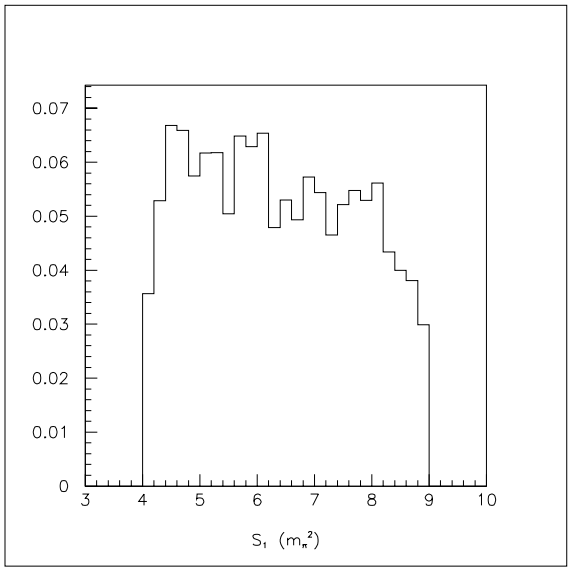

Figure 10: S_1 acceptance for 700 MeV incident photons.

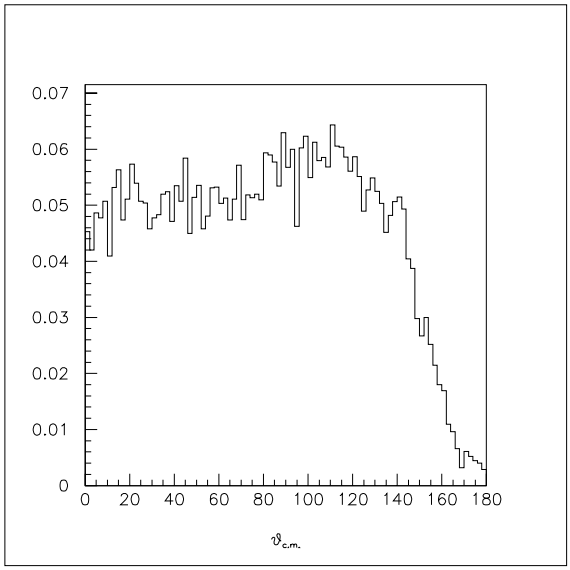

Figure 11: Dependence of the acceptance on the center-of-mass photon scattering angle for 700 MeV incident photons, $-t = 0.5 - 6$ and $S_1 = 4 - 9$.

5.4 Statistics

The event rate is estimated directly from the cross section for a pure $t-$channel process. The value of $\alpha + \beta$ is taken as 0.0 fm^3, and the value of $\alpha - \beta$ is taken as 0.0014 fm^3. The total $\gamma\pi$ center mass cross section is obtained by integrating Eq. 5 from 0 to 40 degree. The overall γp cross section is calculated by using Eq. 10.

To estimate precision, we assume the starting photon energy $E_0 = 500 MeV$ and the one month total counts are obtained by scaling up to 1000 MeV according to the dependence on the photon beam energy by

$$N(t, S_1) = N_T F T \sigma(E_0, t, S_1) E_0^2 \sum_{i=0}^{500} \frac{1}{(E_0 + i\delta)^2},$$

where N_T is the number of protons per cm^2, F is the effective incidental photon flux per energy bin δ which is taken as 1 MeV, T is the running time (one month) in seconds, and $\sigma(E_0)$ is the cross section at the starting energy and within the center mass angle from 0 to 40 degree.

With 3.2 GeV electron beam and 5 cm long liquid hydrogen target at a luminosity of $10^{34} cm^{-2} sec^{-1}$, the equivalent photon flux will be 6×10^5 /MeV/s in the energy range 500 to 1000 MeV. The detector acceptance is taken as 7% in average, which includes a 10% neutron detection efficiency and 70% acceptance of CLAS. With the above setting, we obtain the event numbers listed in Table 2; the last column is the estimated statistical error for the cross section in the corresponding t region. With one month run time, the statistics at each t-bin can reach the 2% level. It should be noted, the above estimation covers only the 500 to 1000 MeV range and θ_{cm} from 0 to 140°. Including data for other kinematics as well as from higher values of S_1, the anticipated precision could be much higher.

The above estimation is made for forward scattering angles only, with a proper upgrade of a forward angle π^+ detector, backward angle scattering data could also be obtained simultaneously. Possibly, we could have measurements of both $\alpha + \beta$ and $\alpha - \beta$ in one experiment. This would put a more stringent constraint on models.

$-t\backslash S_1$	4.5	5.5	6.5	7.5	8.5	sum	ϵ_σ (%)
.50	835.	773.	737.	715.	699.	3759.	1.631
1.50	902.	834.	796.	772.	755.	4060.	1.569
2.50	767.	710.	677.	656.	642.	3453.	1.702
3.50	650.	601.	574.	556.	544.	2924.	1.849
4.50	940.	869.	829.	804.	786.	4229.	1.538
5.50	822.	761.	726.	704.	688.	3701.	1.644
6.50	730.	675.	644.	625.	611.	3285.	1.745
7.50	656.	606.	579.	561.	549.	2951.	1.841

Table 2: Overall event numbers for $\theta_{cm} = 0 - 40^\circ$ and incident $500 - 1000$ MeV photons in one month beam time.

5.5 Backgrounds

For this experiment the two main sources of background will be from the $\gamma p \to \pi^+ n$ and $\gamma p \to \pi^\circ \pi^+ n$ reactions. Events from the one-pion production reaction can be rejected by applying a cut in missing energy. This reaction has only two particles in the final state and these will be confined to a narrow band in a plot of E_{π^+} versus θ_{π^+}, whereas events from the $\gamma p \to \pi^+ n \gamma$ reaction of interest, will be spread out over a larger phase space. Due to the $\approx 1\%$ energy resolution for measuring the π^+ and the neutron, events having a missing energy of less than 10 MeV, corresponding approximately to the threshold of the calorimeter, should, in principle, be readily distinguishable from two-pion production events provided these are not overwhelmingly abundant. Measurements at Mainz[39] of the total cross section for $\gamma p \to \pi^\circ \pi^+ n$ show it to be 46.5 μb at 779 MeV, roughly 500 times larger than the 0.09 μb cross section predicted for $\gamma p \to \gamma \pi^+ n$. However, at Mainz the total cross section was measured, whereas the $\gamma p \to \gamma \pi^+ n$ cross section is a partial cross section, with kinematic cuts in t, S_1 and photon scattering angle $\theta_{\gamma\gamma}^{\rm cm}$. Thus recourse must be made to theory in order to fairly compare the two cross sections. For photon energies near 700 MeV the model of Gomez *et al.*[41] underestimates the observed total $\gamma p \to \pi^\circ \pi^+ n$ cross section by about a factor of two. In contrast, calculations by Ochi *et al.*[40], shown in Fig. 12, are in better agreement with experiment and these are therefore preferred for our purposes. The results of Ochi indicate that the restriction of t and S_1, as well as the π^+ and neutron angles to 30°-80° and 20°-50°, respectively as is appropriate for the three-body kinematic distribution, leads to a partial cross section roughly two orders of magnitude smaller than the total $\gamma p \to \pi^\circ \pi^+ n$ cross section for photon energies above 700 MeV. Thus we anticipate that, with the same kinematic cuts, the background $\gamma p \to \pi^\circ \pi^+ n$ cross section should be only several times larger than the $\gamma p \to \gamma \pi^+ n$ reaction of interest. As indicated by Fig. 13, at this level the two reactions can be cleanly separated. Of course, a further reduction of backgrounds can be achieved when scattered photons are detected in the electromagnetic shower counters, as will occur for much of the phase space.

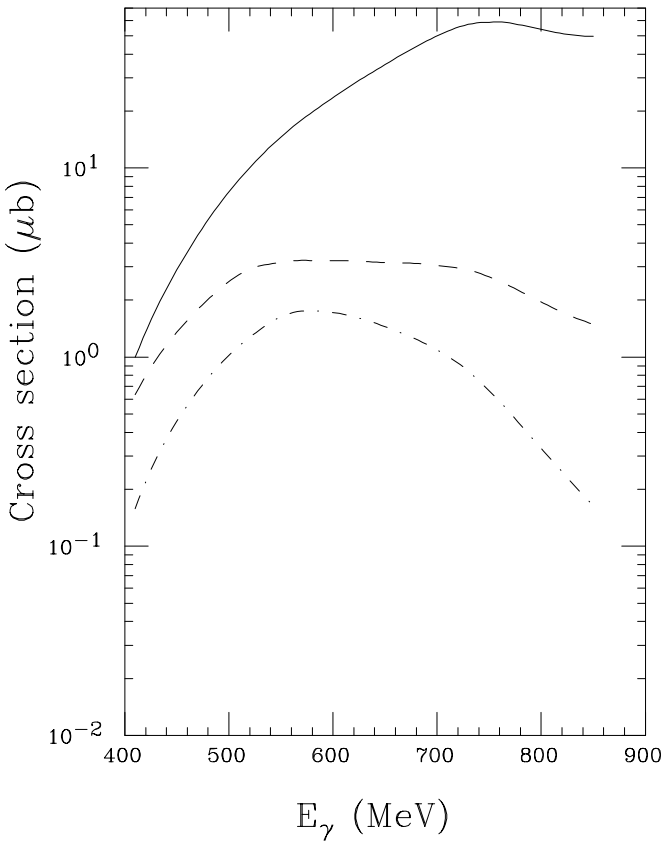

Figure 12: Cross section for two-pion production, calculated by Ochi[40]. The solid curve is the total cross section; dashed curve is for $|t| < 6$ and $9 > S_1 > 4$; and dash-dotted curve includes the additional constraints the angles of the π^+ and neutron are restricted to $30° - 80°$ and $20° - 50°$, respectively.

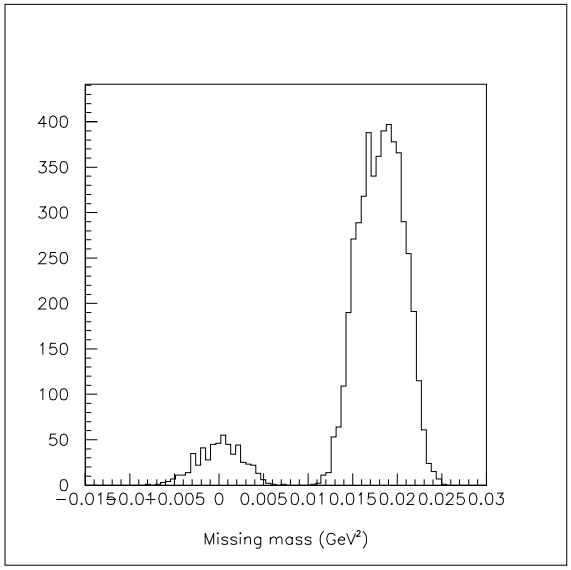

Figure 13: Missing mass spectrum for the $\gamma p \rightarrow \pi^\circ \pi^+ n$ reaction with an unobserved π°. The calculations are for 700 MeV photons, $-t = 2.5$, $S_1 = 6.0$, and $\theta^{\rm cm}_{\gamma\gamma} = 20^\circ$. The number of π° production events was assumed to be ten times than photon scattering events.

5.6 Comparison with Other Experiments

As previously noted, a new series of experiments have been proposed to study Compton scattering from pions. For example, the $\gamma\gamma \to \pi\pi$ reaction constitutes part of the core research program of the DaΦne collider, recently commissioned in Frascati. The 2nd DaΦne handbook[42] contains detailed consideration about what the $\gamma\gamma \to \pi\pi$ reaction can say regarding pion polarizabilities. As previously indicated, this subject has generated considerable controversy. Nevertheless, the conclusion is expressed, *within the* DaΦne *handbook*, that whereas there are good reasons for measuring $\gamma\gamma \to \pi\pi$ reaction, *it is not a means by which one should attempt to determine the pion polarizability.*

A separate experimental effort[28][29] is approved at Mainz to measure the pion polarizability using radiative photoproduction, the same reaction we seek to exploit at JLab. This experiment has an advantage over the proposed JLab investigation in that the the Mainz investigation will employ an array of BaF_2 crystals capable of measuring the scattered photons with an energy resolution of $3 - 5\%$, about four times better than CLAS can achieve. At Mainz, produced pions will be detected using a forward planes of multi-wire proportional chambers, and, as with the JLab proposal, neutrons are to be measured by TOF scintillators. While this detector configuration provides versatility lacking in CLAS, it does not have the comprehensive acceptance CLAS offers. In particular, because their detectors are restricted in their solid angle coverage, the Mainz experiment is configured to measure exclusively the backward-angle photon scattering that is sensitive to the polarizability difference. It is projected that $\bar{\alpha} - \bar{\beta}$ will be determined with an extrapolation uncertainty of approximately 3×10^{-4} fm^3. A determination of the sum $\bar{\alpha} + \bar{\beta}$ would require a different detector set-up, and this has not been proposed.

Additional differences distinguish the JLab and Mainz experiments. At Mainz it is intended to utilize photons from the high-rate GEM tagging facility[43] that is presently under development. While this facility has the potential to tag photons at rates up to 3×10^8 Hz, it utilizes a bremsstrahlung radiator and hence a large flux of untagged photons will be directed on the target. Consequently, backgrounds will be more difficult to deal with than at

CLAS. Moreover, the photon beam tagged by GEM will be unpolarized, and hence, as with the more restricted detector acceptance, there is no capability of using this tool as a means for ensuring the reliability of the extrapolation to the pion pole. To summarize, we consider the Mainz and JLab studies to be complementary. The versatility of the relatively simple Mainz set-up permits a determination of the polarizability difference. The JLab experiment would be sensitive to the polarizability sum, and provide the extensive detector acceptance that is critical for testing the systematics of the extrapolation needed to determine Compton scattering from the pion.

The COMPASS[44] collaboration at CERN also includes a determination of the polarizability of the pion among its broad range of goals. To be commissioned in 1999, COMPASS will employ a fixed targets and beams of muons, pion, kaons, and protons with momenta up to 300 GeV/c. Particles will be detected by the forward magnetic spectrometers that include drift-chamber tracking and lead-glass calorimetry. RICH counters provide particle identification, and the electronics feature dedicated triggers and fast read-out. The polarizability of the pion will be determined[45] from the Primakoff process of pion scattering from virtual photons in the field of a heavy nucleus. Kaon polarizabilities will likewise be investigated using kaon beams. In the meson rest frame, the equivalent energy of incident photons ranges from 100-2000 MeV. These studies rely upon the identification of the Primakoff cross section by means of its strong peaking at very small t. Similar to the cross section measured in radiative photoproduction, the Primakoff cross section is mainly given by the Thomson term, but also contains contributions from the electric and magnetic polarizabilities that vary according to the photon scattering angle $\theta_{\gamma\gamma}^{cm}$ in the meson rest frame. Values for both $\bar{\alpha}$ and $\bar{\beta}$ may be extracted by fitting data over the full range of $\theta_{\gamma\gamma}$ angles that COMPASS has access to. It is projected[45] that for a COMPASS pion beam rate of 5 MHz about 2×10^6 Primakoff events per month should be observed, yielding polarizabilities with statistical uncertainties of the order of 0.2, considerably better than will be achieved in the proposed JLab experiment.

Perhaps the main concern regarding the COMPASS experiment are backgrounds, for example the high rate of non-interacting beam pions that enter the forward spectrometer. The Primakoff trigger is designed to reject this background. Although several other backgrounds[46], both strong and elec-

tromagnetic, are also present, these do not display the low-t peaking that is the signature of the Primakoff process. As a result, most backgrounds can be assessed by extrapolating to low-t their contributions observed at higher t. What is important then is the relative size of the Primakoff and background contributions at low-t, but this remains to be established.

In the absence of a free pion or photon target, there is no experimentally clean means of determining pion polarizability. All experimental methods are subject to appreciable backgrounds, and, polarizability generally provides only a small correction to the Compton cross section. Consistency between the results of various experiments is essential for a satisfactory experimental understanding of pion polarizability. Experimentally, radiative pion photoproduction and radiative pion scattering are subject to different types of backgrounds, and the analysis procedures also differ. Hence consistency between these two methods would serve to establish experimental values for pion polarizability that are on a much more secure footing.

6 Summary

We seek one month of beam time in order to investigate the polarizabilities of the charged pion. Our method relies upon pion photoproduction using the proposed low Q^2 electroproduction photon source. The combination of the polarized photon source and the CLAS detector is particularly well-suited for a determination of the sum of the electric and magnetic pion polarizabilities, $\bar{\alpha} + \bar{\beta}$. Indeed, ChPT makes firm predictions, for up to four pion loops, that $\bar{\alpha} + \bar{\beta} = 0$ and $\bar{\alpha} - \bar{\beta} = 5.6 \times 10^{-4} fm^3$. A six-loop calculation yields $\bar{\alpha} + \bar{\beta} = 0.3 \times 10^{-4}\text{fm}^3$. A one-month run using CLAS will permit us to test these predictions to a precision of better than $1 \times 10^{-4}\text{fm}^3$, an improvement of almost one-order of magnitude over the only previous experimental determination of the polarizability sum of derived from radiative pion scattering as well as for the polarizability difference. This would permit us to make a needed check of the convergence properties of ChPT.

In addition, a modest improvement of the forward angle pion detector would enable us also to measure $\alpha - \beta$.

The polarizabilities of the pion have heretofore resisted precise determination. Experiments are in the planning stages at a number of laboratories, but none of these experiments will be easy. Nevertheless, by means of a multi-pronged attack that draws upon the diverse strengths of different facilities, we can expect that the experimental situation regarding the pion polarizabilities will be significantly improved during the next few years. At CLAS we have a real opportunity to contribute to this progress.

References

[1] V. Bernard and W. Weise, Phys. Lett. **B159**, 85 (1988).

[2] V. Bernard and D. Vautherin, Phys. Rev. **D40**, 1615 (1989).

[3] V. Petrun'kin, Sov. J. Part. Nucl. **12**, 278 (1981).

[4] L. Fil'kov *et al.*, Phys. Rev. **D26**, 3146 (1982).

[5] D. Babusci *et al.*, Phys. Lett. **B277**, 158 (1992).

[6] B. Holstein, Comm. Nucl. Part. Phys. **19**, 221 (1990).

[7] B. Holstein, Nucl. Phys. **A546**, 213 (1992).

[8] A. L'kov and V. Petrun'kin, JETP Lett **37**, 63 (1983).

[9] J. Gasser and H. Leutwyler, Nucl. Phys. **B250**, 465 (1985).

[10] J. Donoghue and B. Holstein, Phys. Rev. **D40**, 2378 (1989).

[11] V. Bernard and W. Weise, Phys. Lett. **238**, 111 (1990).

[12] K. Kawarabayashi and M. Suzuki, Phys. Rev. Lett. **16**, 255 (1966).

[13] Riazuddin and Fayyazuddin, Phys. Rev. **147**, 1071 (1966).

[14] M. Ivanov and T. Mizutani, Phys. Rev. **D45**, 1580 (1992).

[15] G. Chew *et al.*, Phys. Rev. **106**, 1345 (1957).

[16] H. Primakoff, Phys. Rev. **31**, 899 (1951).

[17] D. Drechsel and L. Fil'kov, Z. Phys. **A349**, 177 (1994).

[18] T. Aibergenov *et al.*, Czech. J. Phys. B **36**, 948 (1986).

[19] Y. M. Antipov *et al.*, Phys. Lett. **121B**, 445 (1983).

[20] Y. M. Antipov *et al.*, Z. Phys. **C26**, 495 (1985).

[21] C. Berger *et al.*, Z. Phys. **C26**, 199 (1984).

[22] A. Courau *et al.*, Nucl. Phys **B271**, 1 (1986).

[23] Z. Ajaltoni *et al.*, DM2 Coll, VII Int. workshop on photon-photon collision, Paris, 1986.

[24] J. Boger *et al.*, Phys. Rev. **D42**, 1350 (1990).

[25] H. Marsiskie *et al.*, Phys. Rev. **D42**, 1350 (1990).

[26] Kaloshin94, Phys. Atom. Nucl. **57**, 2207 (1994).

[27] J. Portoles and M. Pennington, The Second DaΦne handbook INFN-Laboratori Nazionali di Frascati http://hpteor.lnf.infn.it/dafne.html, 1995.

[28] J. Ahrens *et al.*, Few-Body Systems, Supl **9**, 449 (1995).

[29] J. Ahren *et al.*, Preprint of Lebdev Phys. Inst., 1996.

[30] Kowalewski *et al.*, Phys. Rev. **D29**, 1000 (1984).

[31] L. Fil'kov and V. Kashevarov, Eur. Phys. J **A5**, 285 (1999).

[32] R. Walker *et al.*, High Energy Phys., Proc. Ann. Rochester **10**, 17 (1960).

[33] P. Cziffra *et al.*, Nucl. Phys. **36**, 258 (1962).

[34] G. Smith *et al.*, Phys. Rev. Lett. **5**, 571 (1960).

[35] R. Miskimen, K. Wang, and A. Yegneswaran, CEBAF Proposal, 94-015, 1994.

[36] T. Aibergenov *et al.*, Proc. of the Lebedev Phys. Inst. **186**, 169 (1988).

[37] A. Afanasev *et al.*, Internal report, 2002.

[38] B. Niczyporuk, private communication, SDA code, 1995.

[39] A. Braghieri *et al.*, Phys. Lett. **B363**, 46 (1995).

[40] K. Ochi *et al.*, private communication and LANL preprint nucl-th/9703058 and nucl-th/9711031, 1997.

[41] J. G. Tejedor and E. Oset, Nucl. Phys **A600**, 413 (1986).

[42] The Second DaΦne handbook INFN- Laboratori Nazionali di Frascati http://hpteor.lnf.infn.it/dafne.html, 1995.

[43] I. Anthony *et al.*, Nucl. Instrum. and Meth. **A301**, 230 (1991).

[44] Common Muon and Proton Apparatus for Structure and Spectroscopy; CERN/SPSLC 96-14 http://www.compass.cern.ch/compass/proposal/, 1996.

[45] M. A. Moinester and V. Steiner, Proc. of the CERN COMPASS Summer School, Prague, Czech Republic, Aug. 1997 (hep-ex/9801011), 1997.

[46] M. A. Moinester, Pion and Sigma Polarizabilities and Radiative Transitions, in Chiral Dynamics: Theory and Experiment, Ed. A. Bernstein and B. Holstein, Springer-Verlag (hep-ph/9409463), 1994.